AUTONOMOUS FORMATION FLIGHT USING BIFURCATING POTENTIAL FIELDS

Masayuki Suzuki, Kenji Uchiyama
Department of Aerospace Engineering, Nihon University

Keywords: *UAV, Formation Flight, Swarm, Artificial Potential Field, Bifurcation*

Abstract

This paper attempts to design a guidance law using bifurcating potential fields for a swarm of autonomous Unmanned Aerial Vehicles (UAVs). We consider an autonomous flight system that can create different swarming patterns so as to guarantee obstacle and vehicle collision avoidance. The guidance law, which is derived from a steering and repulsive potential field, can express variable geometric patterns for a formation flight of UAVs. The system can transition between different formation patterns by way of a simple parameter change. Numerical simulation is performed to verify the validity of the proposed guidance law.

1 Introduction

A flight system using multiple Unmanned Aerial Vehicles (UAVs) has recently attracted interest for applications such as scientific data collection and reconnaissance for civil or military purposes. Flight control systems have been studied [1-5] in order to achieve more advanced applications that cannot be achieved by means of a single UAV. However, guidance and control laws become more complex as the number of UAVs increases.

Artificial potential fields have been applied to the design of controllers for swarming systems [5-11]. The basic concept behind this theory is to create a workspace in which each UAV is attracted toward an equilibrium state, the stability of which is generally guaranteed by Lyapunov's second method. However, the control system may become complex for the case in which the goal state is allowed to vary during a mission. Bennet and McInnes have applied classical bifurcation theory to the potential field to overcome this problem [4, 5]. Their method, which is simple and can be quickly executed, can allow for different configurations to be formed through a simple parameter change of the potential function.

Several methods using artificial potential fields have been proposed in recent years with regard to formation control [12-15]. Most of these methods use artificial potential fields simply to avoid collisions and for guidance to a desired position. In the present paper, we expand the previous guidance method using bifurcating potential field so as to be able to achieve a three-dimensional flight configuration by applying a new technique for using artificial potential. The goal of the present study is to develop a guidance method for a mission, such as three-dimensional formation flying of UAVs, and to verify the validity of the newly developed guidance method through numerical simulations.

2 Formation Flying

2.1 Guidance Law

Figure 1 shows the inertial coordinate system *o-xyz* and position vectors of the UAVs.

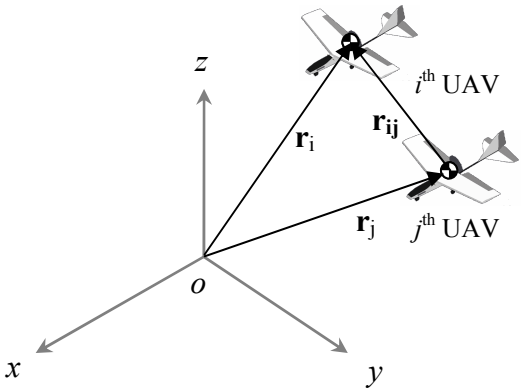

Fig. 1. Definition of position vectors

We consider a swarm of homogeneous UAVs, which are treated as particles, each of which interacts via a velocity field $\mathbf{v}_i$ (i =1, …, n) using a steering potential F^S and a repulsive potential F^R governed by the following equation:

$$\mathbf{v}_i = -\nabla_i F^S(\mathbf{r}_i) - \nabla_i F_{ij}^R(\mathbf{r}_{ij}) . \quad (1)$$

The desired command speed, heading angle, and pitch angle of each UAV are then obtained as follows:

$$v_{d,i} = \sqrt{v_{x,i}^2 + v_{y,i}^2 + v_{z,i}^2} , \quad (2)$$

$$\psi_{d,i} = \tan^{-1}\left(\frac{v_{y,i}}{v_{x,i}}\right), \quad (3)$$

$$\theta_{d,i} = \tan^{-1}\left(\frac{v_{z,i}}{v_{x,i}}\right), \quad (4)$$

where $v_{x,i}$, $v_{y,i}$, and $v_{z,i}$ are the axial components of the desired command speed $v_{d,i}$.

The desired roll angle command $\phi_{d,i}$ is defined as follows:

$$\phi_{d,i} = K_\psi(\psi_i - \psi_{d,i}), \quad (5)$$

where K_ψ is the gain of the roll angle command, and ψ is the heading angle.

The steering potential [4] F^S is defined as follows:

$$F^S(\rho_i) = \mu C_e \exp\left(\frac{-(\rho_i - \rho_d)^2}{L_e}\right) + C_h\left(\sqrt{(\rho_i - \rho_d)^2 + 1} + \sqrt{\sigma_i^2 + 1}\right), \quad (6)$$

where C_h represent the amplitude of the hyperbolic potential function, μ is the bifurcation parameter, C_e and L_e represent the amplitude and length scales, respectively, of the exponential potential function, and ρ and σ are the parameters of the desired formation pattern, as denoted by subscript d. We define ρ_i so as to be able to form a ring or line formation and σ_i so as to be able to form a three-dimensional formation by the following equations:

$$\rho_i = \begin{cases} \sqrt{x_i^2 + y_i^2 + z_i^2} \ \textit{for ring formation} \\ x_i \ \textit{or} \ y_i \ \textit{or} \ z_i \ \textit{for line formation} \end{cases}, \quad (7)$$

$$\sigma_i = ax_i + by_i + cz_i , \quad (8)$$

where a, b, and c represent the vector components of σ_i.

Three-dimensional formation flying can be achieved by manipulating parameters a, b, and c which can change the angle of the formation pattern. If a = 1, b = 0, and c = 0, then a formation pattern that is parallel to the y-z plane is generated. In the case of a = 1, b = 1, and c = 1, a formation pattern that is inclined at an angle of 45 degrees to the x-y, y-z, and z-x planes is generated.

Depending on the value of μ, the steering potential can change the positions of stationary points and take on various forms. Figures 2(a) and 2(b) show examples of the velocity field when μ is negative and positive, respectively.

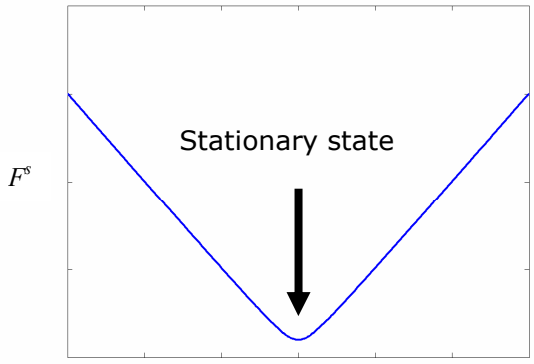

(a) $\mu < 0$

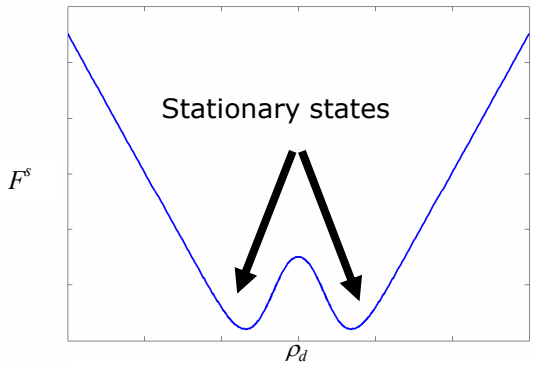

(b) $\mu > 0$

Fig. 2. Bifurcating potential field

In particular, the steering potential has one state of dynamical equilibrium at a desired distance ρ_d, as shown in Fig. 2(a) when the

parameter μ is negative. On the other hand, when μ is positive, the steering potential has two stationary states, as shown in Fig. 2(b).

These results imply that the formation pattern can be changed easily through manipulation of the parameters μ, ρ, a, b, and c.

The repulsive potential [16] is defined in as follows:

$$F_{ij}^{R} = C_r \sum_{j,j\neq i} \exp\left(-\frac{|\mathbf{r}_{ij}|}{L_r}\right), \tag{9}$$

where C_r and L_r represent the amplitude and length scales of the repulsive potential function, respectively, and $|\mathbf{r}_{ij}| = |\mathbf{r}_i - \mathbf{r}_j|$.

The total repulsive bound velocity on the i^{th} UAV is dependent on the position of the other (n-1) UAVs in the formation. The repulsive potential is therefore used to ensure that the UAVs do not collide with each other as they are steered toward the goal state.

In applying the proposed methods, it is important that the stability of the system be determined in order to ensure that the described behaviors will occur. In order to determine the stability of the system, we consider two methods, namely, Lyapunov's Second Theorem and an eigenvalue analysis of the linearized equations of motion. [4, 5] The results of this analysis indicate that the system can always be considered to be stable.

2.2 Control Law

In order to achieve steady-state flight, we use a robust controller for a linear time-invariant multi-variable system [17]. We can express the state and output equations for longitudinal and lateral motions, which are linearized around the equilibrium point, as follows:

$$\dot{\mathbf{x}}(t) = \mathbf{A}\mathbf{x}(t) + \mathbf{B}\mathbf{u}(t), \tag{10}$$

$$\mathbf{y}(t) = \mathbf{C}\mathbf{x}(t). \tag{11}$$

First, we define the error $\mathbf{e}(t)$ between output $\mathbf{y}$ and input $\mathbf{y}_d$ (see Fig. 3), as shown in the following equation:

$$\boldsymbol{e}(t) = \boldsymbol{y} - \boldsymbol{y}_d. \tag{12}$$

By differentiating Eq. (10), we obtain

$$\frac{d}{dt}\dot{\mathbf{x}}(t) = \mathbf{A}\dot{\mathbf{x}}(t) + \mathbf{B}\dot{\mathbf{u}}(t). \tag{13}$$

If the system is in a steady state, then we can assume that $\dot{\boldsymbol{y}}_d = \mathbf{0}$, and

$$\frac{d}{dt}\mathbf{e}(t) = \mathbf{C}\dot{\mathbf{x}}(t). \tag{14}$$

By combining Eqs. (13) and (14), we obtained the expanded system:

$$\frac{d}{dt}\begin{bmatrix}\dot{\boldsymbol{x}}(t)\\ \boldsymbol{e}(t)\end{bmatrix} = \begin{bmatrix}\boldsymbol{A} & \boldsymbol{0}\\ \boldsymbol{C} & \boldsymbol{0}\end{bmatrix}\begin{bmatrix}\dot{\boldsymbol{x}}(t)\\ \boldsymbol{e}(t)\end{bmatrix} + \begin{bmatrix}\boldsymbol{B}\\ \boldsymbol{0}\end{bmatrix}\dot{\boldsymbol{u}}(t). \tag{15}$$

In order to stabilize this system, we consider the rank of the matrix in the following equation:

$$rank\begin{bmatrix}\mathbf{A} & \mathbf{B}\\ \mathbf{C} & \mathbf{0}\end{bmatrix} = n + p, \tag{16}$$

where n is the order of matrix $\mathbf{A}$, and p is the number of outputs. Accordingly, we can control only two variables for both the longitudinal and lateral equations, and we choose U and θ for longitudinal motion, and ϕ and ψ for lateral motion to control speed and attitude. The control input $\mathbf{u}$ for longitudinal and lateral motions of this system is given by the following equation:

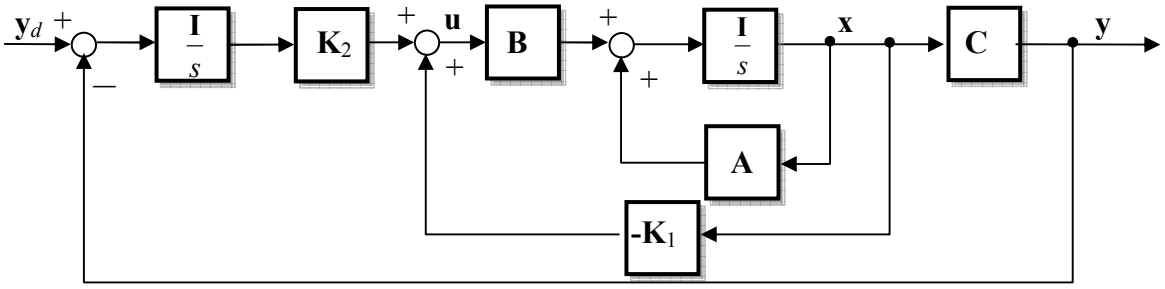

Fig. 3. Block diagram of the controller of the linear time-invariant multi-variable system

$$\mathbf{u}(t) = -\mathbf{K}_1\mathbf{x}(t) - \mathbf{K}_2\int_0^t \mathbf{e}(t)dt\,, \qquad (17)$$

where $\mathbf{K_1}$ and $\mathbf{K_2}$ are the feedback gains of this controller.

In addition, if the system is in transition, $\dot{\mathbf{y}}_d$ is not constant. However, we can control the system toward input $\mathbf{y}_d$, because the poles of the system never change, despite $\dot{\mathbf{y}}_d \neq \mathbf{0}$.

3 Numerical Simulations

3.1 UAV Dynamics

Figure 4 shows the block diagram of the entire system using proposed guidance and control laws. To simulate swarm control of the UAVs, we used a model [18] for the UAV that is linearized about straight and level flight conditions with a forward speed of 12.5 m/s and θ_0 = 0.00 rad. Equations (18) and (19) show the longitudinal and lateral equations of motion, respectably. Figure 5 shows the definitions of the state variables and control inputs.

$$\frac{d}{dt}\begin{bmatrix} U \\ W \\ q \\ \theta \end{bmatrix} = \begin{bmatrix} X_u & X_w & 0 & -g\cos\theta_0 \\ Z_u & Z_w & U_0 + Z_q & -g\sin\theta_0 \\ M_u & M_w & M_q & 0 \\ 0 & 0 & 1 & 0 \end{bmatrix}\begin{bmatrix} U \\ W \\ q \\ \theta \end{bmatrix} + \begin{bmatrix} X_{\delta e} & X_{\delta t} \\ Z_{\delta e} & Z_{\delta t} \\ M_{\delta e} & M_{\delta t} \\ 0 & 0 \end{bmatrix}\begin{bmatrix} \delta_e \\ \delta_t \end{bmatrix}, \qquad (18)$$

$$\frac{d}{dt}\begin{bmatrix} V \\ p \\ r \\ \phi \\ \psi \end{bmatrix} = \begin{bmatrix} Y_v & Y_p & Y_r - U_o & g\cos\theta_0 & 0 \\ L_v & L_p & L_r & 0 & 0 \\ N_v & N_p & N_r & 0 & 0 \\ 0 & 1 & \tan\theta_0 & 0 & 0 \\ 0 & 0 & 1 & 0 & 0 \end{bmatrix}\begin{bmatrix} V \\ p \\ r \\ \phi \\ \psi \end{bmatrix} + \begin{bmatrix} Y_{\delta a} & Y_{\delta r} \\ L_{\delta a} & L_{\delta r} \\ N_{\delta a} & N_{\delta r} \\ 0 & 0 \\ 0 & 0 \end{bmatrix}\begin{bmatrix} \delta_a \\ \delta_r \end{bmatrix}, \qquad (19)$$

where U, V, W, p, q, r, ϕ, θ, and ψ are variables and, δ_t, δ_a, δ_r, and δ_e are deflections of moving surfaces from trim conditions. Tables 1 and 2 show the linearized parameters of longitudinal and lateral motions, respectively. The subscripts denote the partial derivatives with respect to the parameters.

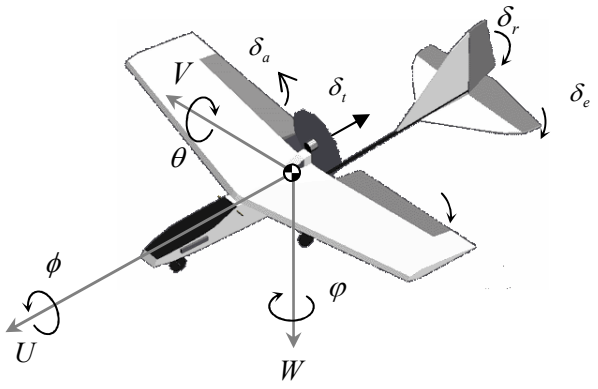

Fig. 5. Definitions of state variables and control inputs

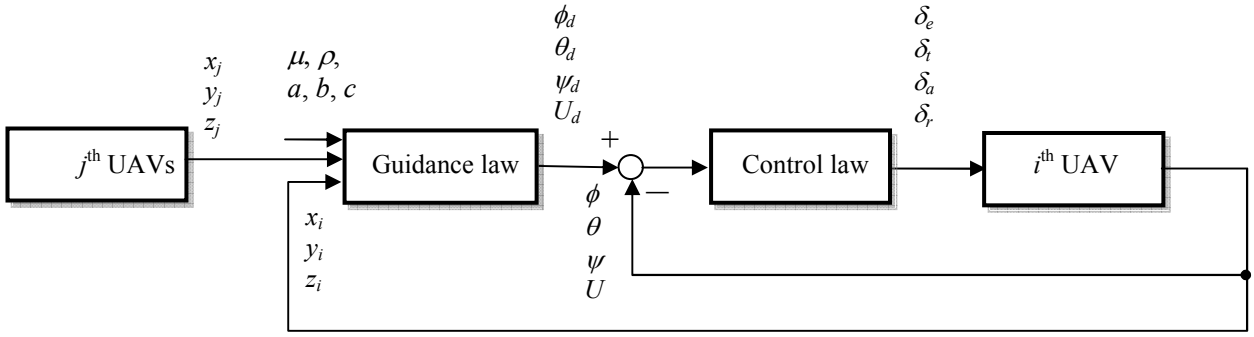

Fig. 4. Block diagram of the entire system

Table. 1. Linearized parameters for longitudinal motion

X_U	[s^{-1}]	-0.13
X_W	[s^{-1}]	0.14
Z_U	[s^{-1}]	-3.17
Z_W	[s^{-1}]	-13.06
Z_q	[m s^{-1}]	1.37
U_o	[m]	12.5
M_U	[$m^{-1}s^{-1}$]	-1.95
M_W	[$m^{-1}s^{-1}$]	-17.41
M_q	[s^{-1}]	-21.86
$X_{\delta e}$	[m s^{-2}]	0
$X_{\delta t}$	[kg^{-1}]	2.32
$Z_{\delta e}$	[m s^{-2}]	-7.73
$Z_{\delta t}$	[kg^{-1}]	0
$M_{\delta e}$	[s^{-2}]	-205.25
$M_{\delta t}$	[s^{-2}]	0

Table. 2. Linearized parameters for lateral motion

Y_V	[s^{-1}]	-0.68
Y_p	[m s^{-1}]	-0.11
Y_r	[m s^{-1}]	-12.20
L_V	[m^{-1} s^{-1}]	-32.17
L_p	[s^{-1}]	-56.38
L_r	[s^{-1}]	19.30
N_V	[m^{-1} s^{-1}]	7.89
N_p	[s^{-1}]	-3.13
N_r	[s^{-1}]	-4.00
$Y_{\delta a}$	[m s^{-2}]	-3.34
$Y_{\delta r}$	[m s^{-2}]	22.99
$L_{\delta a}$	[s^{-2}]	-26.88
$L_{\delta r}$	[s^{-2}]	-6.80
$N_{\delta a}$	[s^{-2}]	58.46
$N_{\delta r}$	[s^{-2}]	-226.79

3.2 Simulation Results

A numerical simulation is performed to verify the validity of the proposed guidance and control laws. We can generate different formations, single line, double line, single ring, double ring, and cluster formations in any plane by using the potential functions. The line and ring formations position UAVs along a line and on a circumference of the circle. The double line formation lines up the UAVs in a row, and the double ring formation positions UAVs in concentric circles. These formations can be formed with different dimensions by changing a parameter of hyperbolic and exponential potential function. The cluster formation positions the UAVs equidistantly based on the parameters of the repulsive potential. Three-dimensional formation flying can be achieved by manipulating parameter σ.

Table. 3. Parameters of potential functions (line)

t	0-50	50-100
μ	1	0
ρ_d	0	0

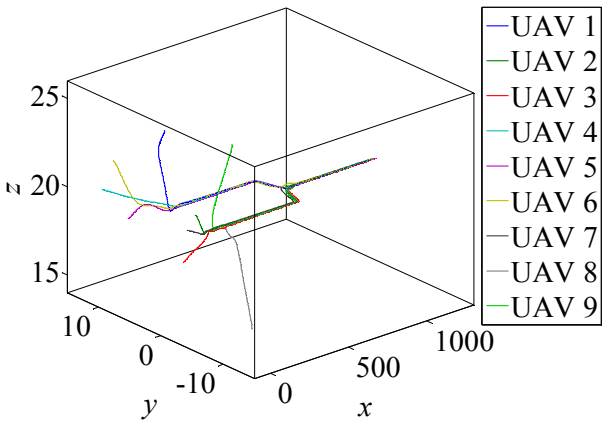

Fig. 6. Flight trajectories

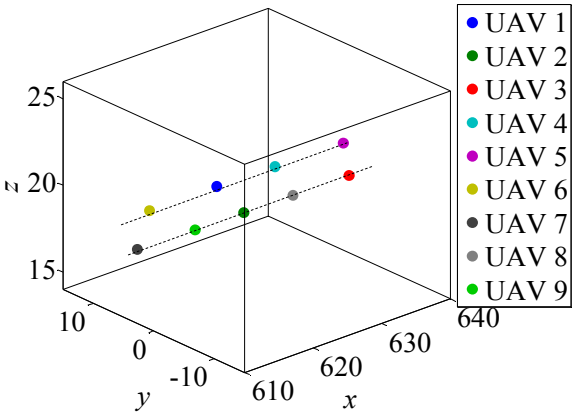

Fig. 7. Double line (t = 50)

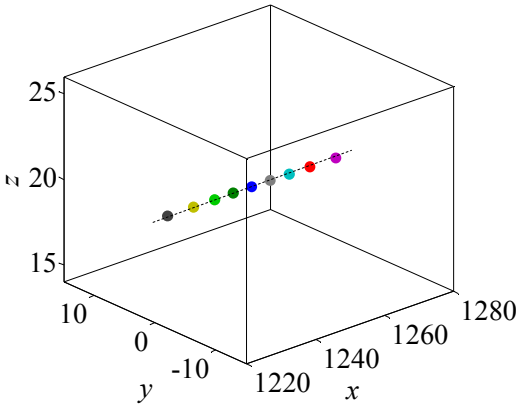

Fig. 8. Single line (t = 100)

Figures 6 through 12 show the transition of a formation of nine UAVs flying with no wind. Figures 6 through 8 show the transition of a line formation. Figures 9 to 12 show the transition of a ring formation. The poles of the controller are placed at -5.5, the simulation parameters are set to $C_r = 2$, $L_r = 4$, $C_h = 1$, $C_e = 6$, $L_e = 6$, $a = 0$, $b = 0$, $c = 1$, and the values of the other parameters of the potential functions F^S are listed in Tables 3 and 4. Figure 6 shows the case in which the system changes from a double line to a single line. In addition, Fig. 9 shows the case in which the system changes from a double ring to a single ring to a cluster every 50 s, whereby each UAV attains the desired position. This is achieved through a simple parameter change and is one of the advantages of using a bifurcation equation as the basis for the artificial potential functions, because we do not need to control each UAV individually.

Figures 13 through 18 show the three-dimensional transition of a formation of nine UAVs. The poles of the controller are placed at -5.5, and the simulation parameters are set to $C_r = 2$, $L_r = 2$, $C_h = 1$, $C_e = 6$, $L_e = 6$, $\mu = 0$, and $\rho_d = 10$. Through this numerical simulation, we changed parameters a, b, and c, as shown in Table 5, every 50 s. Figures 14 through 18 show that the formation transitions from a ring in the x-y plane to a ring in y-z plane by rotating the formation 45 degrees.

Figure 19 shows the UAVs speed, the angular velocity, the Euler angles, and the control inputs throughout the three-dimensional transition. The saturation limits for the aircraft control surfaces are $\delta_e = \pm 0.35$ rad and δ_a, $\delta_r = \pm 0.79$ rad, and the thrust range is $-0.35 < \delta_t < 5.45$ N. The controller is within its limits because the maximum control velocity was determined using a hyperbolic potential function.

Figure 20 shows the time responses of the controlled variables of the UAV. These results reveal that each variable followed the commands satisfactorily.

Table. 4. Parameters of potential functions (ring)

t	0-50	50-100	100-150
μ	1	0	0
ρ_d	10	10	0

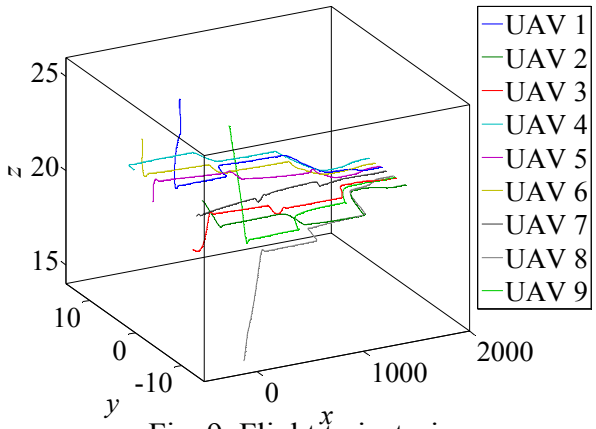

Fig. 9. Flight trajectories

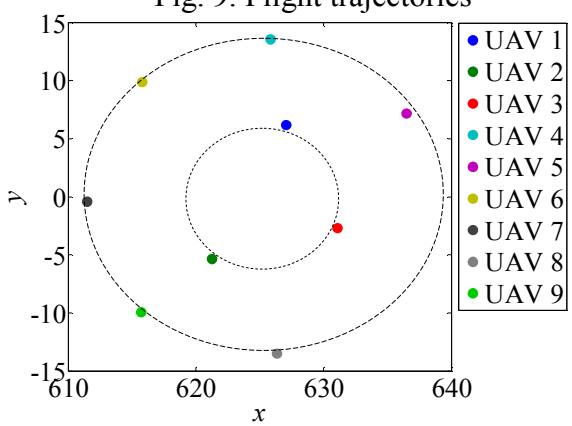

Fig. 10. Double ring ($t = 50$)

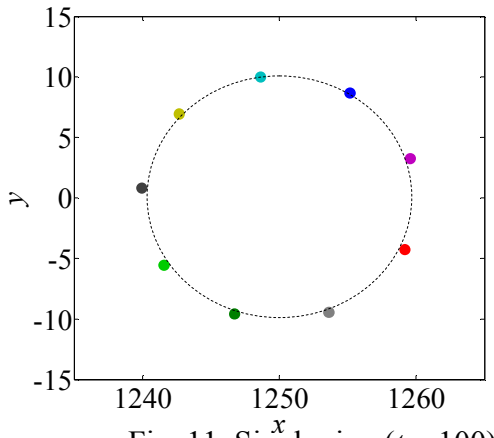

Fig. 11. Single ring ($t = 100$)

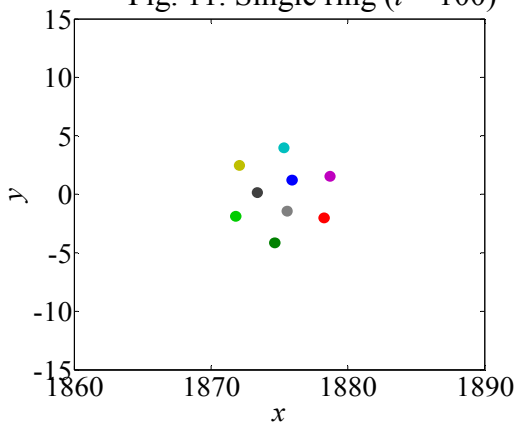

Fig. 12. Cluster ($t = 150$)

Table. 5. Parameters of potential functions

t	0-50	50-100	100-150	150-200	200-250
a	0	0	0	1	1
b	0	1	1	1	0
c	1	1	0	0	0

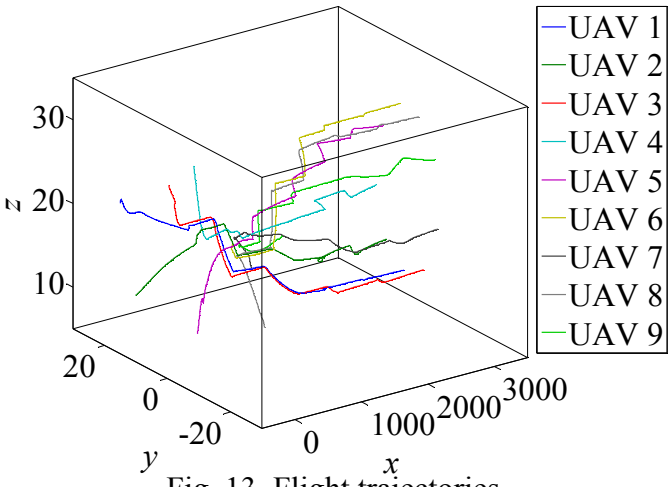

Fig. 13. Flight trajectories

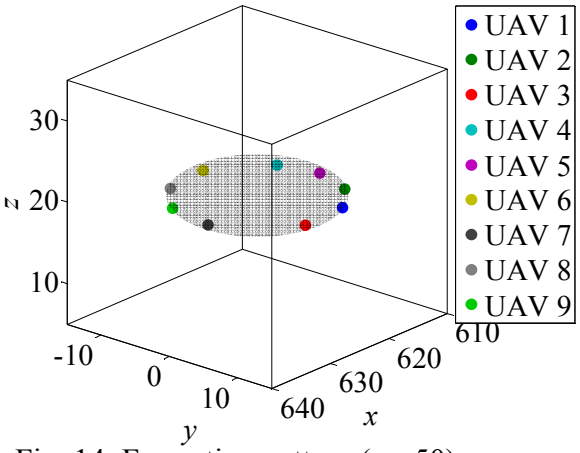

Fig. 14. Formation pattern (t = 50)

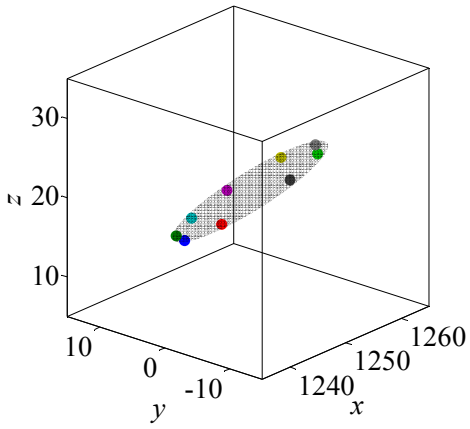

Fig. 15. Formation pattern (t = 100)

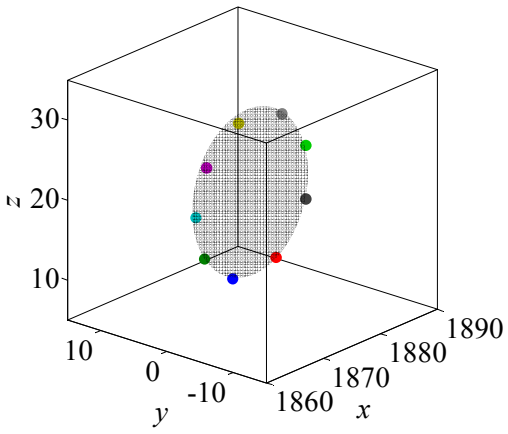

Fig. 16. Formation pattern (t = 150)

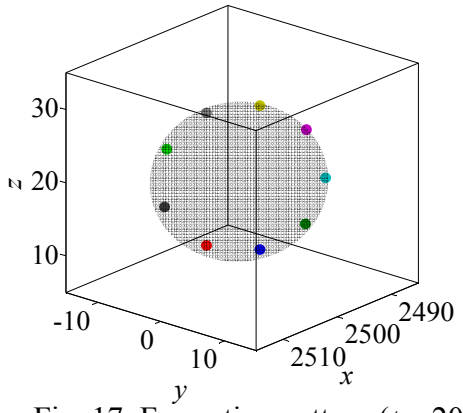

Fig. 17. Formation pattern (t = 200)

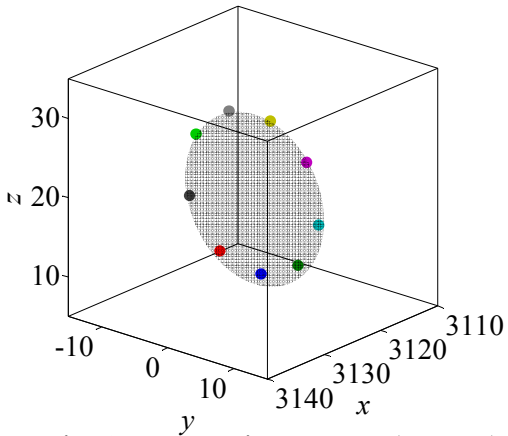

Fig. 18. Formation pattern (t = 250)

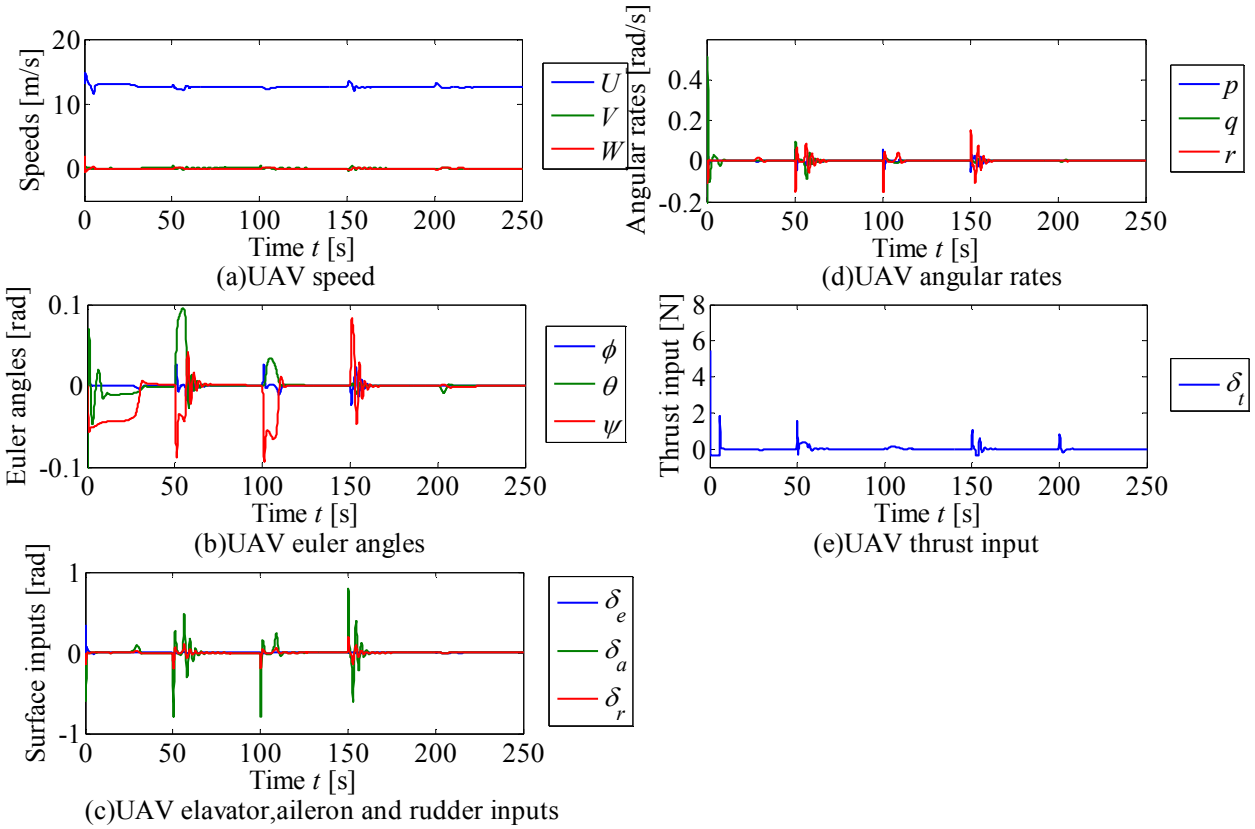

Fig. 19. Time histories of speed, angular rate, Euler angles, and inputs (UAV 1)

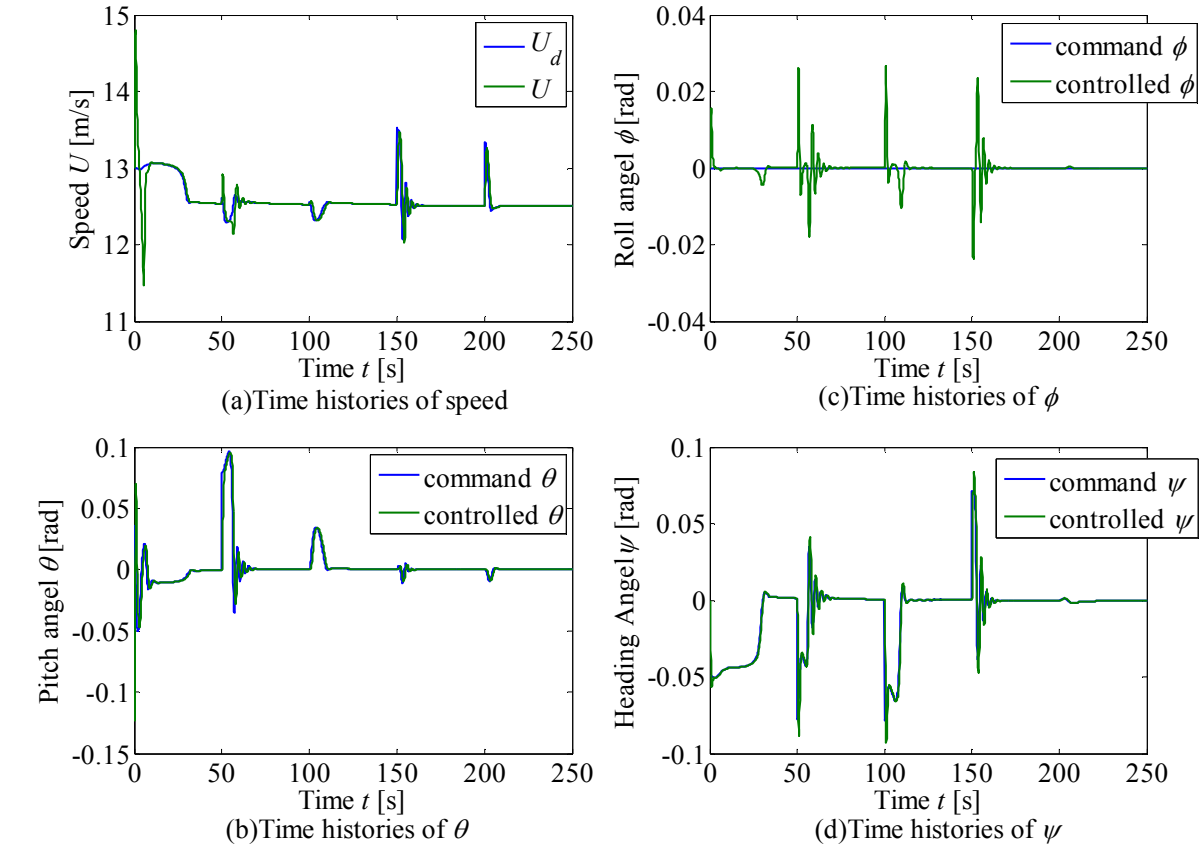

Fig. 20. Time histories of speed and Euler angles (UAV 1)

4 Conclusions

In the present paper, we have described a newly proposed guidance law that uses a new approach involving an artificial potential field and the bifurcation theory. The proposed guidance law can change formation patterns three-dimensionally through simple parameter changes. Numerical results verified the validity of the guidance and control law based on the potential function method for formation flying of UAVs.

References

[1] Gu Y, et al. Design of Flight Testing Evaluation of Formation Control Laws. IEEE Transaction on Control Systems Technology, Vol. 14, No. 6, 2006, pp. 1105-1112.

[2] Ryoo C K, Kim Y H and Tahk M J. Optimal UAV Formation Guidance Laws with Timing Constraint. *International Journal of Systems Science*, Vol. 37, No. 6, pp. 415-427, 2006.

[3] Kim S and Kim Y. Three Dimensional Optimum Controller for Multiple UAV Formation Flight Using Behavior-based Decentralized Approach. *International Conference on Control, Automation and Systems*, pp. 1387-1392, 2007.

[4] Lee J, et al. Formation Geometry Center based Formation Controller Design using Lyapunov Stability Theorem. *2008 KSAS-JSASS Joint International Symposium*, pp. 614-618, 2008.

[5] Paul T, Krogstad T R and Gravdahl J T. Modeling of UAV Formation Flight Using 3D Potential Field. *Simulation Modeling Practice and Theory*, Vol. 16, Issue 9, pp. 1453-1462, 2008.

[6] Shimada Y, Uchiyama K, et al. Proximity Maneuver and Obstacle Avoidance Control Using Potential Function Guidance Method. *Proceedings of International Symposium on Space Technology and Science*, pp. 557-562, 2006.

[7] McInnes C R. Potential Function Methods for Autonomous Spacecraft Guidance and Control. *Adv. Astronaut Sci.,* Vol. 90, No. Pt.2, 1996, pp. 2093-2109.

[8] McInnes C. R. Velocity field path-planning for single and multiple unmanned aerial vehicles. *The Aeronautical Journal*, Vol. 107, No. 1073, pp. 419-426, 2003.

[9] Bennet D and McInnes C R. Spacecraft Formation Flying Using Bifurcating Potential Fields. *International Astronautical Congress*, IAC-08-C1.6.4, 2008.

[10] Bennet D and McInnes C R. Pattern Transition in Spacecraft Formation Flying via The Artificial Potential Field Method and Bifurcation Theory. *3rd International Symposium on Formation Flying, Missions and Technologies*, 2008.

[11] Huang W H, Fajen B R, Fink J R and Warren W H. Visual Navigation and Obstacle Avoidance Using a Steering Potential Function. *Robotics and Autonomous Systems*, 54, pp. 288-299, 2006.

[12] Kowalczyk W and Kozlowski K. Artificial Potential Based Control for a Large Scale Formation of Mobile Robots. *Proceedings of the Fourth International Workshop on Robot Motion and Control*, pp. 285-291, 2004.

[13] Yan Y and Zhang Y. Collision avoidance Planning in Multi-robot based on Improved Artificial Potential Fields and Rules. *International Conference on Robotics and Biomimetics Bangkok,* Thailand, pp. 1026-1031, 2009.

[14] Li K, Han X and Qi G. Formation and Obstacle-Avoidance control for Mobile Swarm Robots Based on Artificial Potential Field. *International Conference on Robotics and Biomimetics,* China, pp. 2273-2277, 2009.

[15] Barnes L, Fields M and Valavanis K. Unmanned Ground Vehicle Swarm Formation Control Using Potential Fields. *Mediterranean Conference on Control and Automation*, Athens-Greece, pp. 1-8, 2007.

[16] D'Orsogna M R, Chuang Y L, Bertozzi A L and Chayes L S. The Road to Catastrophe: Stability and Collapse in 2D Driven Particle Systems. *Physical Review Letters*, Vol. 96, No. 10:14302-1, 2006.

[17] Davison E. The robust control of a servomechanism problem for linear time-invariant multivariable systems. *Automatic Control, IEEE Transactions on*, 21(1), pp. 25–34, 1976.

[18] Hyslop A M and Humbert J S. Wide-field integration methods for autonomous navigation of 3-D Environments. *AIAA Guidance, Navigation, and Control Conference and Exhibit*, 2008-7252:1–18, 2008.

Copyright Statement